February 2005 • NREL/CP-520-37338

Conference Paper

AFM-Based Microelectrical Characterization of Grain Boundaries in Cu(In,Ga)Se_2 Thin Films

C.-S. Jiang, R. Noufi, K. Ramanathan,
J.A. AbuShama, H.R. Moutinho, and
M.M. Al-Jassim

Prepared for the 31st IEEE Photovoltaics Specialists Conference and Exhibition
Lake Buena Vista, Florida
January 3–7, 2005

National Renewable Energy Laboratory
1617 Cole Boulevard, Golden, Colorado 80401-3393
303-275-3000 • www.nrel.gov

Operated for the U.S. Department of Energy
Office of Energy Efficiency and Renewable Energy
by Midwest Research Institute • Battelle

Contract No. DE-AC36-99-GO10337

AFM-BASED MICROELECTRICAL CHARACTERIZATION OF GRAIN BOUNDARIES IN $Cu(In,Ga)Se_2$ THIN FILMS

C.-S Jiang, R. Noufi, K. Ramanathan, J. A. AbuShama, H. R. Moutinho, and M.M. Al-Jassim
National Renewable Energy Laboratory (NREL), 1617 Cole Blvd., Golden, CO 80401

ABSTRACT

We report on a direct measurement of two-dimensional potential distribution on the surface of $Cu(In,Ga)Se_2$ thin films using a nanoscale electrical characterization of scanning Kelvin probe microscopy both in air and in ultra-high vacuum. The potential measurement reveals a higher surface potential or a smaller work function on grain boundaries (GBs) of the film than on the grain surfaces. This demonstrates the existence of a local built-in potential on GBs, and the GB is positively charged. The role of the built-in potential in device performance was further examined and found to be positive, by tuning Ga content or band gap of the film. With increasing Ga content, the potential drops sharply in a Ga range of 28%~38%. Comparing the change in the built-in potential to the theoretical and experimental photoconversion efficiencies, we conclude that the potential plays a significant role in the device conversion efficiency of NREL's three-stage $Cu(In,Ga)Se_2$ device.

INTRODUCTION

One of the most surprising achievements for $Cu(In,Ga)Se_2$ (CIGS) polycrystalline solar cell material is its high conversion efficiency (19.2%) [1]. In general, defects in grain boundaries (GBs) in polycrystalline materials form effective recombination centers. However, this is not the case for the CIGS film, in which state-of-the-art cell efficiency of >19% is higher than that demonstrated for single-crystal cells (~13%) [2]. Two controversial arguments on the role of recombination in GBs suggest that the GB is either electrically active or inactive as a recombination center for photogenerated carriers, which may be due to the different GB structures generated by the different fabrication processes of the films [3-5]. However, even if the GB is electrically inactive, this property alone is not sufficient to explain the high performance of the polycrystalline cell compared to its single-crystal counterpart.

A classical model of interface states suggests a local built-in potential around a GB as a result of trapped charges at the interface states on the GB [6]. This local built-in potential can be expected to spatially extend the minority-carrier collection area and thus benefit the photovoltaic effect. However, the deep level of the interface states may also act as recombination centers for the minority carriers, thus reducing their lifetime. In addition, the local built-in potential on the GB does not necessarily exist in all thin-film materials. It remains unclear whether or not the local built-in potential exists on GBs of the CIGS material and whether it plays a positive or negative role in the photovoltaic performance of the device.

In this paper, we report on a direct measurement of the local built-in potential on GBs of CIGS films using a microelectrical characterization technique, namely scanning Kelvin probe microscopy (SKPM). Furthermore, the built-in potential on the GB was examined to be beneficial to photoconversion efficiency of the CIGS devices.

MEASUREMENT TECHNIQUE

We have established the SKPM technique both in air and in ultra-high vacuum (UHV) [7]. SKPM is based on

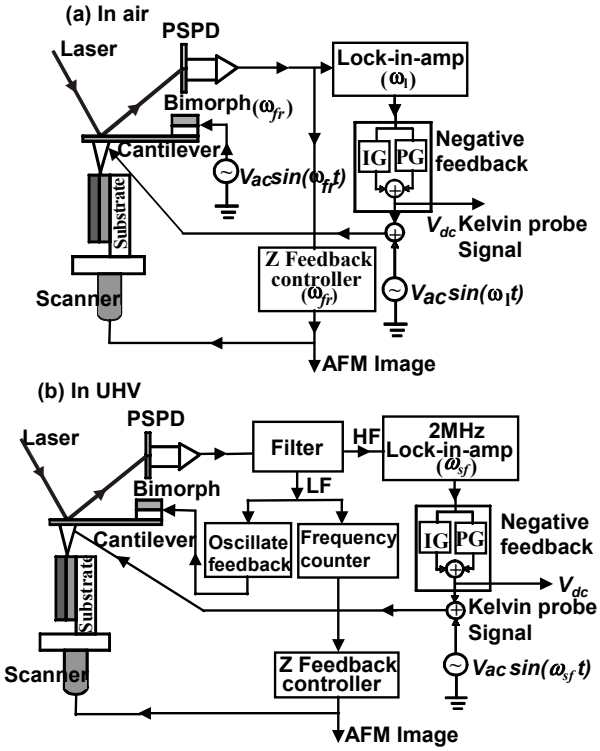

Fig.1. Schematics of SKPM setups (a) in air and (b) in UHV.

the non-contact mode of atomic force microscopy (NC-AFM). Because the resonant oscillation peak of the AFM cantilever is super sharp in UHV (several Hz), amplitude modulation mode of the NC-AFM, which is used in the air-AFM, cannot be used in the UHV-AFM. In contrast to that the cantilever in the air-AFM is driven by an ac voltage at a fixed frequency [$V_{ac}sin(\omega_{fr}t)$ in Fig. 1(a)], the cantilever oscillation in UHV is excited and controlled by a amplifier that keeps the cantilever oscillating at the strongest (the first) resonant oscillation frequency [the "Oscillate feedback" box in Fig. 1(b)]. The real shift of the resonant frequency by the atomic force between the sample surface and the tip is counted and this shift is used to control the Z feedback loop and generate the topographic image. This mode is called frequency modulation of NC-AFM.

Based on the NC-AFM difference between in air and in UHV, the setups of SKPM in air and in UHV are also different. The air-SKPM uses a relatively low frequency ac voltage [$V_{ac}sin(\omega_l t)$ in Fig. 1(a) and $\omega_l \approx$20 kHz] to oscillate the cantilever, and the Coulomb force between the tip and the sample in this frequency can be described by $F(\omega_l) \propto (\phi_s-\phi_t)\ V_{ac}sin(\omega_l t)$, where ϕ_s and ϕ_t are work functions of the sample and the tip and (ϕ_t-ϕ_s) is called contact potential difference. The oscillation in this frequency (note it is different from the frequency $\omega_{fr} \approx$ 70 kHz that is used in probing the sample topography) is detected by the lock-in amplifier, and the detected signal is sent to the negative feedback loop that is applied to the tip. The voltage V_{dc} from the feedback loop is the Kelvin probe signal V_{dc}=(ϕ_t-ϕ_s), because in this case the contact potential difference or the work function difference is compensated by the Kelvin probe signal and the coulomb force $F(\omega_l)$ is zero. Because of the convolution of topography into the Kelvin probe signal, frequency of the ac voltage $\omega_l \approx$20 kHz has to be set far away from the first resonant frequency $\omega_{fr} \approx$70 kHz that is used in probing the topography. The deviation of ω_l from ω_{fr} lowers the energy sensitivity of the potential measurement (~50 mV).

In UHV, because the attenuation of cantilever oscillation in high frequency is not significant, the second resonant frequency [$V_{ac}sin(\omega_{sr}t)$ in Fig. 1(b) and $\omega_{sr} \approx$400 kHz] is used in the Kelvin probe [8], and this enhances the energy sensitivity to ~10 mV. The cantilever oscillation signal is separated to low- and high-frequency components by low- and high-pass filters, and these components are sent to the topographic and the Kelvin probe detection circuits, respectively. Because the second resonant frequency, $\omega_{sr} \approx$400 kHz, is far away from the first resonant frequency, $\omega_{fr} \approx$70 kHz, the convolution of the topography into the Kelvin probe signal is reduced. However, the setup of our UHV-NC-AFM is difficult to scan in a large size (<3 m) on a relatively rough polycrystalline sample (~ 100 nm).

RESULTS AND DISCUSSIONS

The CIGS films being investigated were deposited by NREL's three-stage co-evaporation process on Mo-coated soda lime glass substrates. The film was rinsed in high-purity water before the potential measurement. Water-rinsing was used to remove Na residing on the film surface, which diffused from the soda lime glass substrate onto the surface. The surface Na makes the measured potential peak on the GB broad due to the Na-induced surface dipoles [9]. Figure 2 shows an AFM topographic image of the film surface and the simultaneously obtained SKPM image, measured by the air-SKPM. Comparing the AFM [Fig. 2(a)], SKPM [Fig. 2(b)] images, and the example line profiles [Fig. 2(c)], one see that the electrical potential is higher on the GBs than on the surface of grains. Both topographic and potential images measured in UHV (Fig. 3) are similar to those measured in air (Fig. 2). However, the noise level or the energy resolution is improved in the UHV-SKPM, from ~50 mV to ~10 mV [Fig. 3(c)]. The primary purpose for measuring the potential distribution in UHV is to avoid the effect of air-molecule absorption and surface contamination. However, annealing the sample at 110 °C in UHV for 30 minutes to desorbe water molecules from the sample surface did not significantly change the distribution of the surface potential. Further Ar ion sputtering at 600 V for several

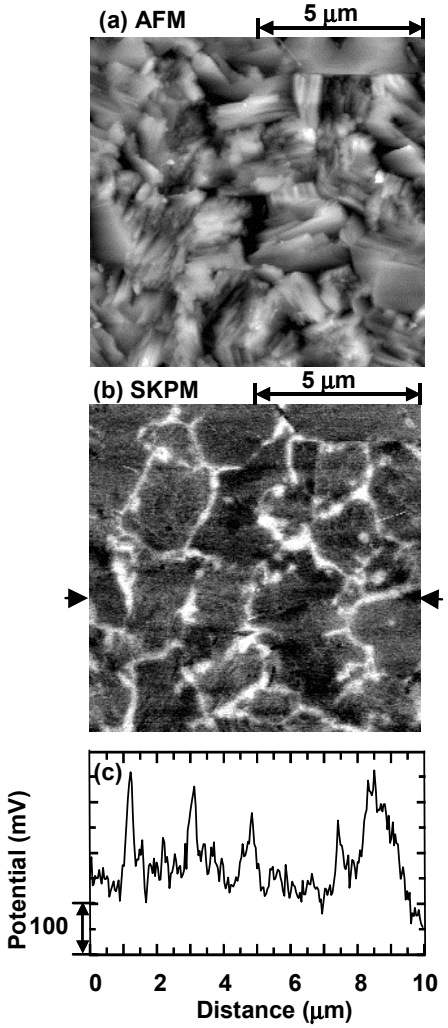

Fig. 2. (a) AFM and (b) the corresponding SKPM images of the CIGS film taken by air-SKPM; (c) a line cut along the arrows in (b).

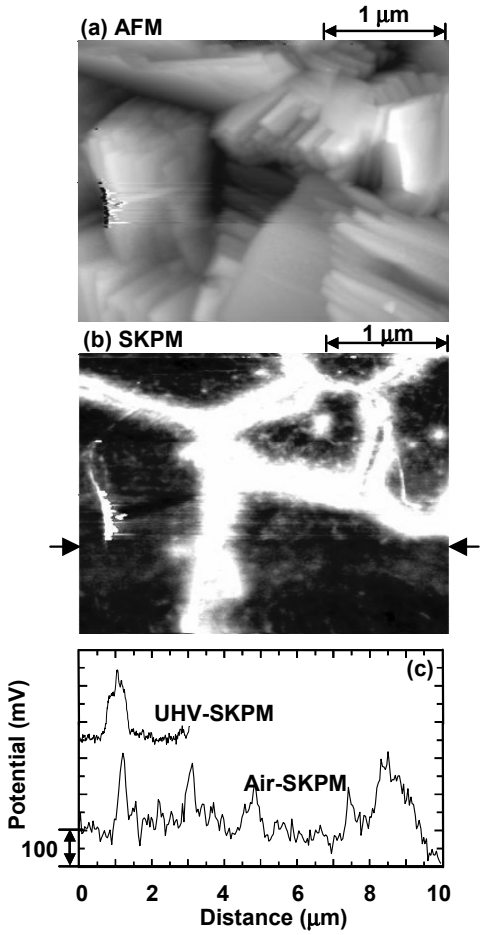

Fig. 3. (a) AFM and (b) the corresponding SKPM images of the CIGS film taken by UHV-SKPM; (c) a line cut along the arrows in (b) together with the line profile in Fig. 2(c) for comparison.

seconds likely damaged the surface structure and caused disappearance of the potential contrast on the GB.

The higher potential on GB demonstrates a downward band bending around the GB in the p-type material [Fig. 4(a)], and that the GB is positively charged. Such local built-in potential makes the local work function smaller on the GB than on the grain surface. Our measured potential height (~150 mV) seems to be small compared to the band gap (~1.15 eV) of CIGS. Most likely, the depletion on the grain surface reduces the contrast of potential between the GB and the grain surface and makes the measured potential peak on the GB smaller than the potential barrier on the GB in the bulk [Fig. 4(b)]. Such surface depletion exists widely on semiconductor surfaces. Therefore, the local built-in potential in the bulk should be between the measured height (~150 mV) and the band gap (~1.15 V).

The local built-in potential on GBs of the CIGS films was further examined to play a significant role in photoconversion efficiency of the device. Band gap of the CIGS films can be tuned from 1.01 to 1.68 eV by adjusting Ga content of Ga/(In+Ga) from 0% to 100% [10]. Although

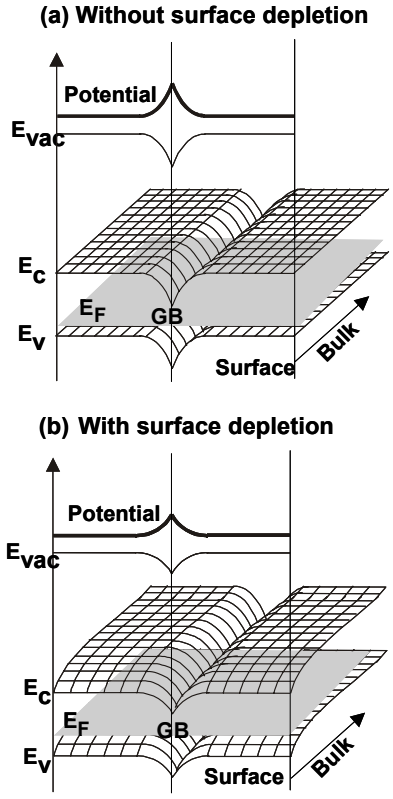

Fig. 4. Schematics of two-dimensional band diagram around the GB in cases of (a) without and (b) with consideration of surface band bending.

a Ga content of ~65% provides the optimal band gap value for optimal conversion efficiency, as theoretically predicted from the solar spectra [11], the actual Ga content in the current record-efficiency device is ~28% [1]. This difference between the theoretical optimal band gap and the experimental Ga content of the highest-efficiency device implies that, in addition to the band gap, other factors play major roles in conversion efficiency. Therefore, identifying the factors that determine conversion efficiency provides an opportunity to address the question of whether the built-in potential on GBs of CIGS film is beneficial to photovoltaic performance.

With varying the Ga content in the film, we found that the potential on the GB drops sharply in a range of 28%~38% Ga [Fig. 5(a)]. The theoretical curve in Fig. 5(b) is predicted solely from the band gap consideration [11]. By comparing the plot of built-in potential in Fig. 5(a) to the theoretical and experimental plots of the conversion efficiency in Fig. 5(b), one sees that the potential on the GB correlates well with the measured device efficiency. The increase of efficiency in the range of 0%~28% Ga is due mainly to the increase of the band gap, and the potential on the GB in this Ga range stays strong. However, at the higher Ga content, the absence of the potential on the GB seems to be significant compared to the effect of the band gap widening. Thus, the drop in the measured efficiency is slower compared to the precipitous drop in the potential at the GB. Even though the

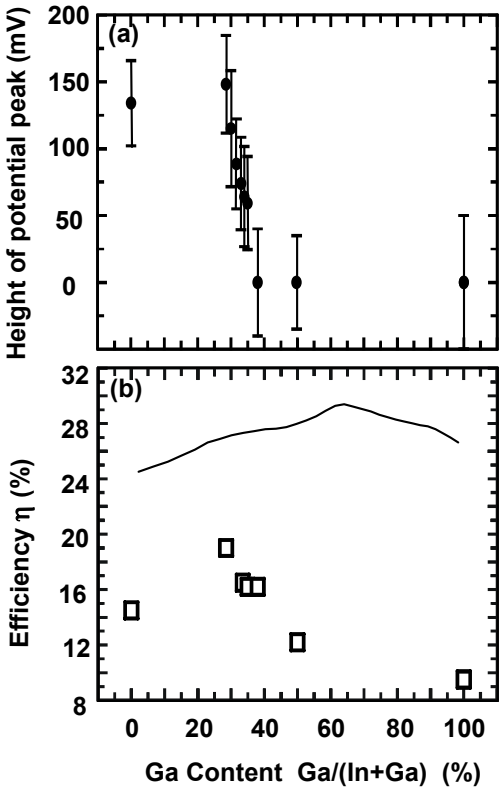

FIG. 5. (a) Measured potential height on the GB versus Ga content of Ga/(In+Ga); (b) Theoretical (solid line) and experimental (squares) conversion efficiencies of CIGS devices versus Ga content.

measured efficiency of a thin-film device is affected by other factors in addition to band gap and built-in potential at the GB, such as the nature of the junction partner and its related band alignment with that of the absorber (e.g., the CIGS in this study), the condition stated above is strong enough to demonstrate a strong benefit of the built-in potential on GBs in thin-film CIGS-based devices.

Although the physics underlying why the GB potential benefits the photovoltaic performance cannot be directly deduced from the potential measurement, a possible mechanism is the GB potential-assisted minority-carrier collection, because the GB potential attracts electrons and repulses holes. If there is a electron path on the GB through the cathode of the device (CdS and ZnO layers) and a hole path in the grain interior through the anode (Mo contact), the potential on the GB can be expected to increase the collection area of minority carriers and change the one-dimensional collection in the p-n junction to a three-dimensional collection configuration. A study of CIGS devices by tuning Ga content pointed out that the low conversion efficiency at high Ga content results mainly from voltage-dependent minority-carrier collection and the low value of fill factor [12], which is consistent with the GB potential-assisted minority-carrier collection mechanism.

CONCLUSIONS

We have demonstrated the existence of local built-in potential at the GB that arises from the positively charged GB, and that the GB potential plays a positive role in device conversion efficiency. This points out an approach for cell design in which the band gap or Ga content is increased while the built-in potential on the GB has to be kept strong. In addition, our finding that the GB potential drops sharply in the Ga range of 28%~38% may open both theoretical and experimental research to investigate what happens to the atomic and electronic structures of the GB in this Ga content.

ACKNOWLEDGEMENT

This work is supported by the U.S. Department of Energy under contract number DE-AC36-99GO10337.

REFERENCES

[1] K. Ramanathan, M. Contreras, C. Perkins, S. Asher, F. Hasoon, J. Keane, D. Young, M. J. Romero, W. Metzger, R. Noufi, J. Ward, and A. Duda, *Prog. Photovolt. Res. Appl.* **11**, 225 (2003).

[2] C. H. Champness, *Proceedings of the 29th IEEE Conference* (IEEE, Piscataway, 2002), P. 732; L. S. Yip and I. Shih, *Proceedings of the 1st World Conference on Photovoltaic Energy Conversion* (IEEE, Piscataway, 1994), P. 210.

[3] B. M. Keyes, P. Dippo, W. K. Metzger, J. AbuShama, and R. Noufi, *J. Appl. Phys*. **94**, 5584 (2003).

[4] O. Lundberg, M. Bodegard, and L. Stolt, *Thin Solid Films* **431-432**, 26 (2003).

[5] K. Bothe, G. H. Bauer, and T. Unold, *Thin Solid Films* **403-404**, 453 (2002).

[6] J. Bardeen, *Phys. Rev*. **71**, 717 (1947).

[7] C.-S. Jiang, H. R. Moutinho, D. J. Friedman, J. F. Geisz, and M. M. Al-Jassim, *J. Appl. Phys*. **93**, 10035 (2003).

[8] A. Kikukawa, S. Hosaka, and R. Imura, *Appl. Phys. Lett*. **66**, 3510 (1995).

[9] C.-S Jiang, R. Noufi, J. A. AbuShama, K. Ramanathan, H. R. Moutinho, J. Pankow, and M.M. Al-Jassim, *Appl. Phys. Lett*. **84**, 3477 (2004).

[10] D. S. Albin, J. J. Carapella, J. R. Tuttle, and R. Noufi, *Mat. Res. Soc. Symp. Proc.* **Vol. 228**, 267 (1992).

[11] M. A. Green, *Solar Cells* (The University of New South Wales, P.O. Box 1, Kensington, NSW 2033, Australia), p. 89.

[12] W. N. Shafarman, R. Klenk, and B. E. McCandless, *Proceedings of the 25th IEEE photovoltaic specialists conference,* 1996, p. 917

REPORT DOCUMENTATION PAGE

Form Approved
OMB No. 0704-0188

PLEASE DO NOT RETURN YOUR FORM TO THE ABOVE ORGANIZATION.

1. REPORT DATE *(DD-MM-YYYY)*	2. REPORT TYPE	3. DATES COVERED *(From - To)*
February 2005	Conference Paper	3-7 January 2005

4. TITLE AND SUBTITLE
AFM-Based Microelectrical Characterization of Grain Boundaries in Cu(In,Ga)Se_2 Thin Film

5a. CONTRACT NUMBER
DE-AC36-99-GO10337

5b. GRANT NUMBER

5c. PROGRAM ELEMENT NUMBER

6. AUTHOR(S)
C.-S. Jiang, R. Noufi, K. Ramanathan, J.A. AbuShama, H.R. Moutinho, and M.M. Al-Jassim

5d. PROJECT NUMBER
NREL/CP-520-37338

5e. TASK NUMBER
PVA53201

5f. WORK UNIT NUMBER

7. PERFORMING ORGANIZATION NAME(S) AND ADDRESS(ES)
National Renewable Energy Laboratory
1617 Cole Blvd.
Golden, CO 80401-3393

8. PERFORMING ORGANIZATION REPORT NUMBER
NREL/CP-520-37338

9. SPONSORING/MONITORING AGENCY NAME(S) AND ADDRESS(ES)

10. SPONSOR/MONITOR'S ACRONYM(S)
NREL

11. SPONSORING/MONITORING AGENCY REPORT NUMBER

12. DISTRIBUTION AVAILABILITY STATEMENT
National Technical Information Service
U.S. Department of Commerce
5285 Port Royal Road
Springfield, VA 22161

13. SUPPLEMENTARY NOTES

14. ABSTRACT *(Maximum 200 Words)*
We report on a direct measurement of two-dimensional potential distribution on the surface of Cu(In,Ga)Se_2 thin films using a nanoscale electrical characterization of scanning Kelvin probe microscopy both in air and in ultra-high vacuum. The potential measurement reveals a higher surface potential or a smaller work function on grain boundaries (GBs) of the film than on the grain surfaces. This demonstrates the existence of a local built-in potential on GBs, and the GB is positively charged. The role of the built-in potential in device performance was further examined and found to be positive, by tuning Ga content or bandgap of the film. With increasing Ga content, the potential drops sharply in a Ga range of 28%~38%. Comparing the change in the built-in potential to the theoretical and experimental photoconversion efficiencies, we conclude that the potential plays a significant role in the device conversion efficiency of NREL's three-stage Cu(In,Ga)Se_2 device.

15. SUBJECT TERMS
PV; AFM-based microelectrical characterization; nanoscale electrical characterization; scanning Kelvin probe microscopy; grain boundaries (GBs); device conversion efficiency;

16. SECURITY CLASSIFICATION OF:			17. LIMITATION OF ABSTRACT	18. NUMBER OF PAGES	19a. NAME OF RESPONSIBLE PERSON
a. REPORT	b. ABSTRACT	c. THIS PAGE			19b. TELEPHONE NUMBER (*Include area code*)
Unclassified	Unclassified	Unclassified	UL		